Immunity
Article

The Membrane Skeleton Controls Diffusion Dynamics and Signaling through the B Cell Receptor

Bebhinn Treanor,[1] David Depoil,[1] Aitor Gonzalez-Granja,[1] Patricia Barral,[1] Michele Weber,[1] Omer Dushek,[2] Andreas Bruckbauer,[1] and Facundo D. Batista[1,*]
[1]Lymphocyte Interaction Laboratory, London Research Institute, Cancer Research UK, 44 Lincoln's Inn Fields, London WC2A 3PX, UK
[2]Sir William Dunn School of Pathology & Centre for Mathematical Biology, University of Oxford, Oxford OX1 3RE, UK
*Correspondence: facundo.batista@cancer.org.uk
DOI 10.1016/j.immuni.2009.12.005

SUMMARY

Early events of B cell activation after B cell receptor (BCR) triggering have been well characterized. However, little is known about the steady state of the BCR on the cell surface. Here, we simultaneously visualize single BCR particles and components of the membrane skeleton. We show that an ezrin- and actin-defined network influenced steady-state BCR diffusion by creating boundaries that restrict BCR diffusion. We identified the intracellular domain of Igβ as important in mediating this restriction in diffusion. Importantly, alteration of this network was sufficient to induce robust intracellular signaling and concomitant increase in BCR mobility. Moreover, by using B cells deficient in key signaling molecules, we show that this signaling was most probably initiated by the BCR. Thus, our results suggest the membrane skeleton plays a crucial function in controlling BCR dynamics and thereby signaling, in a way that could be important for understanding tonic signaling necessary for B cell development and survival.

INTRODUCTION

Adaptive immune responses are initiated after B cell receptor (BCR) recognition of specific antigen on the surface of viruses, bacteria, or presenting cells (Batista and Harwood, 2009). In naive B cells, the BCR is composed of either nonsignaling membrane immunoglobulin M (IgM) or IgD to provide recognition of extracellular antigen, in complex with a signaling transmembrane Igα-β heterodimer containing immunoreceptor tyrosine-based activation motifs (ITAMs) (Reth, 1989). Engagement of specific antigen by the BCR initiates phosphorylation of ITAM residues and the recruitment of intracellular signaling molecules including Vav, Bruton's tyrosine kinase (Btk), phospholipase C-γ2 (PLCγ2), and B cell linker (BLNK) (DeFranco, 1997; Kurosaki, 2002). This intracellular signaling cascade leads to changes in cytosolic calcium concentration and ultimately results in B cell proliferation and differentiation into cells capable of secretion of protective antibodies (Rajewsky, 1996).

Expression of the BCR is absolutely required during B cell development both for positive selection of immature B cells and for survival of mature B cells (Lam et al., 1997; Rajewsky, 1996), suggesting that the BCR transmits a constitutive (tonic) signal. Although the molecular mechanism of tonic signaling remains to be elucidated, it will probably hinge on an understanding of the distribution and behavior of the BCR in the resting B cell membrane. It has been suggested that the BCR exists as oligomers within the resting B cell membrane on the basis of biochemical characterizations (Reth et al., 2000; Schamel and Reth, 2000). Alternatively, fluorescence resonance energy transfer failed to detect any interaction between appropriately labeled Igα and Igβ, indicating that the BCR may exist as a monomer (Tolar et al., 2005). However, the earliest event visualized thus far and associated with successful B cell activation is the formation of signaling BCR microclusters (Depoil et al., 2008; Weber et al., 2008), which is dependent on the Cμ4 domain of the BCR (Tolar et al., 2009). Thus, it is clear that BCR distribution is important for mediating BCR function. In spite of this, very little is known concerning the nature and regulation of BCR diffusion within the plasma membrane.

The diffusion dynamics of both transmembrane and glycosylphosphatidylinositol (GPI)-anchored proteins in the plasma membrane has been investigated via single-particle tracking (SPT) (Kusumi et al., 1993; Saxton, 1993). These studies have led to the postulation that membrane-protein diffusion can be confined within membrane compartments defined by transmembrane protein "pickets" or the membrane-skeleton "fence" (Kusumi et al., 1993, 2005). Within the context of this model, it is likely that the dynamic linkage of the plasma membrane to the underlying actin cytoskeleton influences receptor diffusion and may permit the rapid transitional "hop" diffusion between compartments suggested by the membrane skeleton fence model (Kusumi et al., 2005). One family of proteins that provides a regulated linkage between plasma membrane proteins and the actin cytoskeleton is the widely distributed ezrin-radixin-moesin (ERM) protein family. Phosphorylation of ERM proteins on a threonine within the C-terminal domain induces a conformational opening of the protein to expose a FERM domain in the N terminus and an actin-binding domain in the C terminus (Bretscher et al., 2002). Interestingly in lymphocytes, immunoreceptor signaling induces the rapid and transient dephosphorylation of ERM proteins and their detachment from the actin cytoskeleton (Delon et al., 2001; Faure et al., 2004; Gupta et al.,

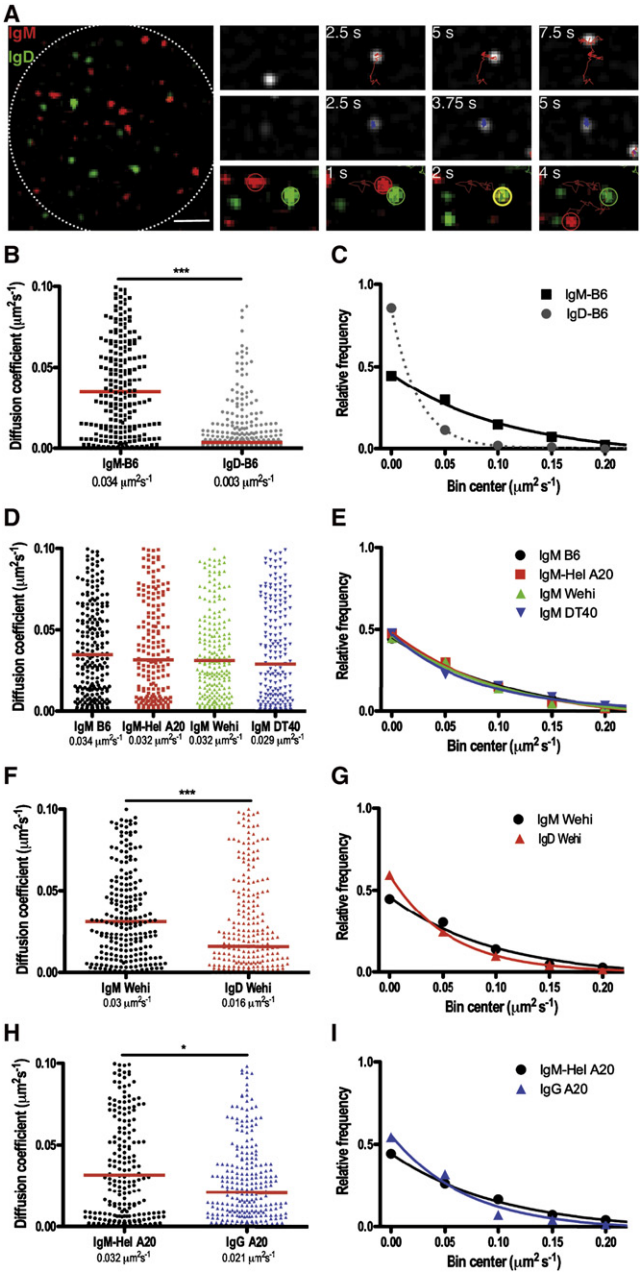

Figure 1. Steady-State BCR Diffusion within the Plasma Membrane Is Restricted

(A–C) Single-molecule tracking of IgM and IgD in primary naive B cells on MHC II-coated coverslips.

(A, top and middle) Different BCR behaviors identified: faster, more mobile diffusion (top, red track) and slower, more confined diffusion (middle, blue track).

(A, bottom) IgM (red) and IgD (green) are occasionally visualized confined in the same volume (yellow circle). Track for IgM is shown (red).

Scale bars represent 2 μm.

(B) Diffusion coefficients of single molecules of IgM (black squares) and IgD (gray circles) with the median indicated in red.

(C) Relative frequencies of single molecules of IgM (black squares) and IgD (gray circles) with diffusion coefficients in the indicated diffusion bins.

(D–I) Steady-state diffusion coefficients (D, F, H) and distribution histogram with diffusion coefficients in the indicated bins (E, G, I) of single molecules of IgM in primary naive B cells adhered to anti-MHC class II-coated coverslips and various B cell lines adhered to fibronectin-coated coverslips (D, E), single molecules of IgM and IgD in the IgM^+IgD^+ Wehi 231 B cell line (F, G), and single molecules of transfected Hel-specific IgM or endogenous IgG in A20 B cells (H, I). ***$p < 0.0001$, *$p = 0.02$.

300 representative diffusion coefficients displayed from a total of 500–3000 from at least two independent experiments. See also Figure S1.

2006) and thus may influence membrane protein diffusion. However, high-resolution imaging of immunoreceptors together with ERM proteins has not been performed.

Early biochemical and electron microscopy studies suggested a link between BCR activation and the actin cytoskeleton (Baeker et al., 1987; Braun et al., 1982; Hartwig et al., 1995; Williams et al., 1994). However, a direct association between the BCR and the actin cytoskeleton in resting cells was not detected. Thus, we have characterized the role and functional significance of the actin cytoskeleton in the regulation of steady-state BCR diffusion. Here, we used high-speed dual-view acquisition total internal reflection fluorescence microscopy (TIRFM) to simultaneously visualize single particles of BCR together with actin and ezrin, a highly conserved member of the ERM family. We show that in resting B cells, actin and ezrin together formed a network that both defined micron-sized compartments containing mobile BCRs and established boundaries to impede BCR diffusion. The efficiency of these actin-defined boundaries to restrict BCR diffusion was largely dependent on the cytoplasmic domain of Igβ. Furthermore, we observed that alteration of the actin network was sufficient to induce robust calcium signaling comparable to that triggered by BCR crosslinking, as well as phosphorylation of downstream signaling molecules and upregulation of activation markers. Moreover, through the use of an extensive panel of B cells deficient in key signaling molecules, we show that this signaling most probably originates from the BCR. Thus, our results suggest that the membrane skeleton plays an important function in controlling BCR dynamics and signaling, thereby implicating the actin cytoskeleton in the control of tonic BCR signaling.

RESULTS

Steady-State BCR Diffusion Is Restricted within the Plasma Membrane

To investigate the regulation of steady-state BCR dynamics, single particles of BCR were visualized via TIRFM in naive B cells under nonstimulatory conditions. Naive B cells express two BCR isotypes, IgM and IgD, so we simultaneously visualized them by labeling with a low concentration of fluorescently labeled anti-IgM- (red) and anti-IgD- (green) specific Fab fragments. As a result, approximately 1 of every 500 BCRs (see Experimental Procedures) on the membrane were labeled. SPT analysis of IgM and IgD revealed that the BCR did not exhibit a single behavior, but rather some single particles of BCR were highly mobile, whereas in other cases, diffusion was largely restricted (Figure 1A; Movie S1 available online). Similar single-molecule behavior for plasma membrane proteins has been described previously (Douglass and Vale, 2005). The size, intensity, and photobleaching of the Fab fragments are characteristic for single molecules (Figure S1), indicating that we are visualizing

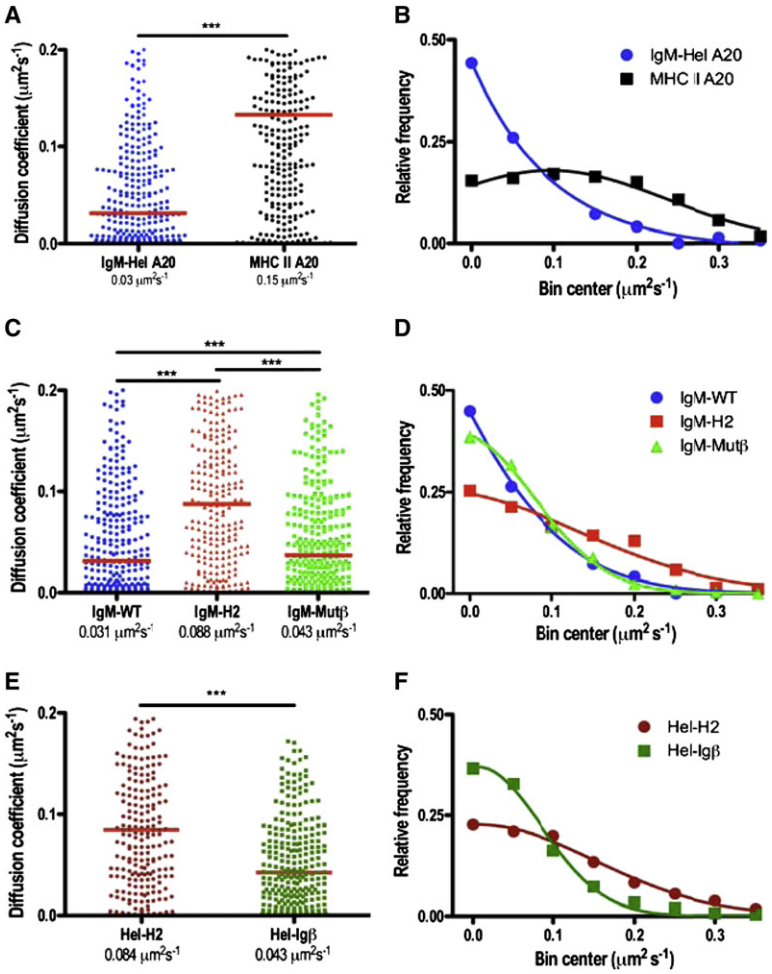

Figure 2. The Cytoplasmic Domain of Igβ Influences Steady-State BCR Diffusion

(A and B) Comparison of the diffusion coefficients (A) and distribution histogram (B) of single molecules of IgM and MHC class II in the A20 B cell line.

(C and D) Single-molecule tracking of chimeric IgM BCRs expressed in A20 B cells.

(C) Diffusion coefficients of single molecules of IgM-WT (blue), IgM-H2 (red), and IgM-Mutβ (green) with median indicated in red.

(D) Relative frequencies of IgM-WT (blue), IgM-H2 (red), and IgM-Mutβ (green) with diffusion coefficients in the indicated bins.

(E and F) Single-molecule tracking of chimeric Hel protein expressed in A20 B cells.

(E) Diffusion coefficients of single molecules of Hel-H2 (red) and Hel-Igβ (green) with median indicated in red.

(F) Relative frequencies of Hel-H2 (red) and Hel-Igβ (green) with diffusion coefficients in the indicated bins.

***$p < 0.0001$. 300 representative diffusion coefficients displayed from a total of 500–3000 from at least three independent experiments. See also Figure S2.

single particles of BCR. The diffusion coefficient can be calculated from the trajectory of individual particles of IgM and IgD. This analysis revealed a wide range of values (Figure 1B), consistent with our observation of different behaviors for individual molecules. Histograms of diffusion coefficients of both IgM and IgD revealed a peak of very slow diffusion coefficients and a trailing shoulder of higher values (Figure 1C). The median diffusion coefficient of IgM was 10-fold greater than that of IgD (0.032 $\mu m^2 s^{-1}$ compared with 0.003 $\mu m^2 s^{-1}$) (Figure 1B). This reflected a nearly 2-fold increase in the slow-diffusing population (left peak of histogram) in IgD compared with IgM (Figure 1C; Movie S1). To determine whether this distribution in diffusion was representative of a general phenomenon in the steady-state lateral diffusion of BCRs in the plasma membrane, we measured IgM diffusion in several cell lines (Figures 1D and 1E). The median diffusion coefficient and the distribution of IgM were consistent between naive and transformed murine B cells as well as chicken B cells. Although to a lesser extent than in primary naive B cells, IgD was slower than IgM in Wehi B cells (Figures 1F and 1G), suggesting some isotype-specific determinants of BCR diffusion. Similarly, IgG diffusion in murine A20 cells was slightly reduced compared to IgM (Figures 1H and 1I). However, the distribution of each of these isotypes exhibited a peak of very slow diffusing BCR and a shoulder of higher values (Figures 1C, 1E, 1G, and 1I).

Thus, it is clear that independent of isotype, a proportion of BCRs exhibit restricted steady-state diffusion within the plasma membrane.

The Intracellular Domain of Igβ Influences BCR Diffusion Dynamics

In contrast to the BCR but consistent with previous reports (Umemura et al., 2008; Vrljic et al., 2002; Wade et al., 1989), major histocompatibility complex class II protein (MHC II) was largely mobile (0.15 $\mu m^2 s^{-1}$ compared with 0.032 $\mu m^2 s^{-1}$; Figure 2A; Movie S2). Indeed, the proportion of slow-diffusing MHC II was less than half that observed for IgM (Figure 2B). This suggests that a BCR-intrinsic factor contributes to the slow-diffusing population of BCRs. Because the diffusion of IgD may be further influenced by the presence of a GPI-linked form of this isotype (Wienands and Reth, 1992), and we are unable to determine the relative number or distinguish between transmembrane and GPI-anchored forms, we have used IgM as a model BCR for further investigation. In order to assess a potential role of the transmembrane and intracellular domains, we tracked single molecules of a chimeric BCR composed of the extracellular domain of IgM fused to the transmembrane and cytoplasmic domain of MHC class I (Williams et al., 1994) (IgM-H2) (Figure S2A). Because naive B cells expressing this chimeric receptor do not undergo allelic exclusion, making IgM-H2 indistinguishable from the endogenous BCR, we expressed it in A20 B cells, which lack endogenous IgM. The median diffusion coefficient of this chimeric receptor was nearly three times faster than that observed for wild-type IgM (0.088 $\mu m^2 s^{-1}$ compared with 0.031 $\mu m^2 s^{-1}$; Figure 2C). This difference was not only a result of the nearly 50% reduction in the proportion of slow-diffusing receptors, but also an increase in the higher values of diffusion coefficient (Figure 2D). Similar values were obtained for MHC class I, consistent with previous reports (Figures S2B and S2C; Edidin et al., 1994; Tang and Edidin, 2003; Vrljic et al., 2005).

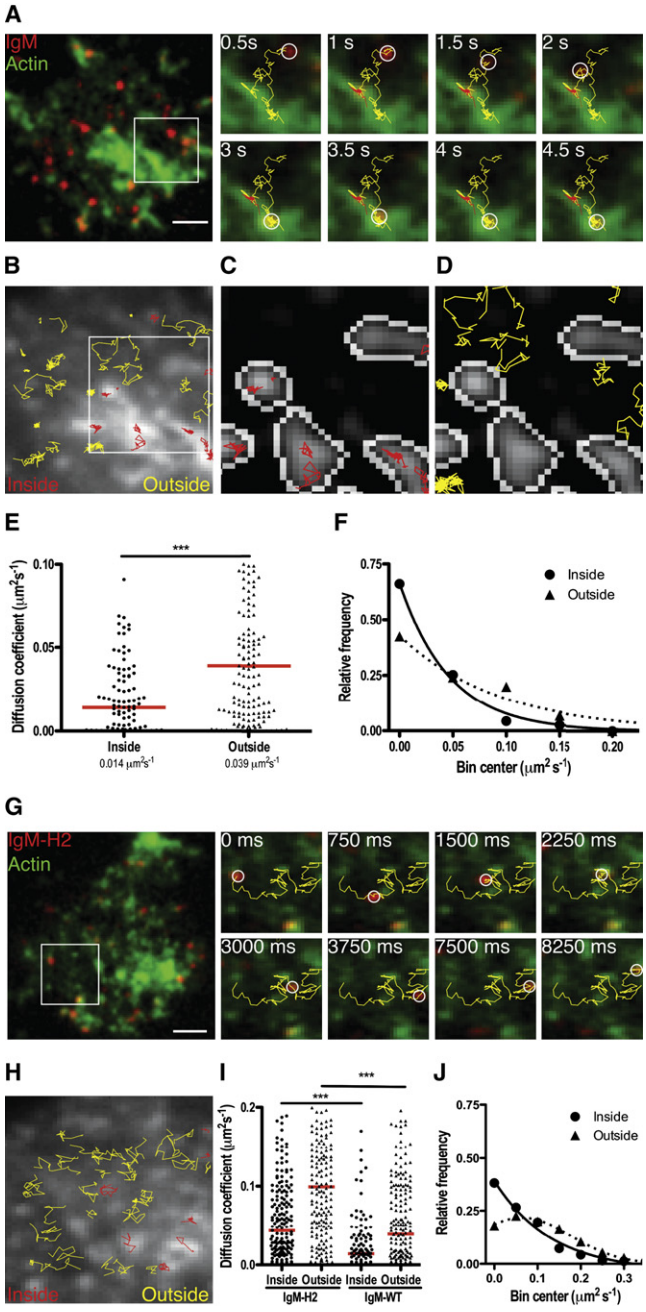

Figure 3. The Actin Cytoskeleton Defines BCR Diffusion Dynamics in Resting B Cells

Dual-view TIRFM to simultaneously visualize Lifeact-GFP (green) and track single molecules of IgM (A–F) or IgM-H2 (G–J) in A20 B cells on fibronectin-coated coverslips.

(A and G) Selected TIRFM images from 200 frame/10 s time sequence at the indicated times during tracking of IgM or IgM-H2 (red). The images in the right panels are magnified time sequences of the left panel (white square) with an example of a 2D trajectory of IgM (A) or IgM-H2 (G) indicated in yellow, with the diffusing particle outlined with a white circle.

(B and H) Magnified image showing trajectories of IgM (B) or IgM-H2 (H) inside (red) and outside (yellow) actin-rich regions (grayscale).

(C and D) Trajectories of IgM inside (C) and outside (D) actin-rich regions, demarcated by white lines.

(E and I) Diffusion coefficients of single molecules of IgM or IgM-H2 inside (circles) and outside (triangles) actin-rich areas with the median indicated by red bar.

(F and J) Relative frequencies of single molecules of IgM (F) or IgM-H2 (J) inside (circles) and outside (triangles) actin-rich areas with diffusion coefficients in the indicated bins.

Scale bar represents 2 μm. ***$p < 0.0001$. 300 representative diffusion coefficients from a total of 500–3000 from at least three independent experiments. See also Figure S4.

Importantly, replacing the intracellular domain of IgM-H2 with the intracellular domain of Igβ (Williams et al., 1994) (IgM-Mutβ) largely restored the diffusion dynamics observed for wild-type IgM (Figures 2C and 2D; Figure S2A). Similar results were obtained for primary naive B cells expressing this chimeric receptor (data not shown). We further verified the importance of the Igβ tail in mediating restricted diffusion by generating chimeric molecules composed of an unrelated protein, the small molecule hen egg lysozyme (Hel), fused to the transmembrane and intracellular domain of MHC class I (Hel-H2), or a similar molecule in which the intracellular domain was replaced with that of Igβ (Hel-Igβ; Figure S2D). The median diffusion coefficient of Hel-H2 was very similar to that observed for IgM-H2 (0.088 $\mu m^2 s^{-1}$ compared with 0.084 $\mu m^2 s^{-1}$; Figures 2E and 2F). Consistent with our previous results, fusion of the intracellular domain of Igβ led to reduced diffusion of the Hel protein (0.043 $\mu m^2 s^{-1}$; Figures 2E and 2F). These results indicate that the intracellular domain of the associated Igβ tail, rather than the transmembrane domain, plays an important role in mediating the restriction in BCR diffusion.

The Actin Cytoskeleton Defines Barriers that Limit BCR Diffusion

The actin cytoskeleton has been implicated in restricting the diffusion of many cell surface proteins (Charrier et al., 2006; Fukatsu et al., 2004; Haggie et al., 2006; Lenne et al., 2006; Sheetz et al., 1980; Suzuki et al., 2005; Wheeler et al., 2007). Furthermore, it has recently been reported that the actin cytoskeleton confines mobile FcεRI in a rat basophilic cell line (Andrews et al., 2008). Because the cytoplasmic domain of Igβ was important for restricting BCR diffusion, we were keen to examine whether this was due to an actin-mediated regulation of BCR diffusion dynamics. We simultaneously visualized the BCR and the actin cytoskeleton in B cells expressing a marker of filamentous actin (F-actin), Lifeact-GFP (Riedl et al., 2008). By using TIRFM we were able to focus our analysis only on the portion of the actin cytoskeleton that is in close proximity to the plasma membrane (~150 nm) and observed an intricate network containing regions of high and low actin density (Figure 3A). We observed that single molecules of BCR exhibiting limited mobility were trapped within regions rich in actin filaments (Figure 3A; Movie S3). In contrast, BCR diffusion was increased within actin-poor areas; however, the boundaries for diffusion tracks within these regions are still defined by the actin network, which appears to act as a diffusion barrier (Figure 3A; Movie S3). Indeed, we observed that mobile single particles of BCR become confined once entering an actin-rich region (Figure 3A; Movie S3). Notably, there was relatively little F-actin reorganization on the time scale of acquisition (10 s), except in peripheral filopodia where linear diffusion of the BCR was

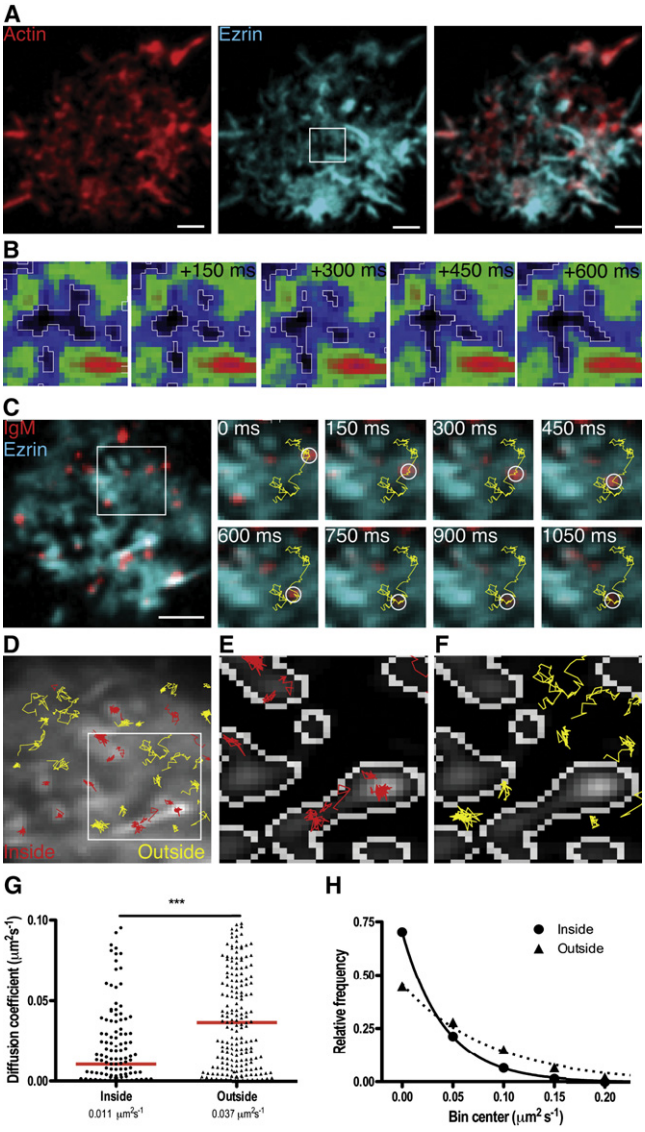

Figure 4. The Membrane Cytoskeleton Linker Protein Ezrin Regulates BCR Diffusion in Resting B Cells

(A) Dual-color TIRFM to visualize the distribution of Lifeact-mRFPruby (red) together with Ezrin-GFP (cyan) in A20 B cells on fibronectin-coated coverslips.

(B) Selected pseudocolor TIRFM images of magnified view of Ezrin-GFP from (A) indicated by white square. Threshold outline (white) shows rapidly modified ezrin "holes."

(C–H) Dual-view TIRFM to simultaneously visualize ezrin-GFP (cyan) and track single molecules of IgM (BCR) in A20 B cells on fibronectin-coated coverslips.

(C) Selected TIRFM images from 200 frames/10 s time sequence at the indicated times during tracking of BCR (red). The images in the right panels are magnified time sequence images of the left panel (white square) with an example of a 2D trajectory indicated in yellow, with the diffusing particle outlined with a white circle.

(D) Magnified image showing 2D trajectories of BCR inside (red) and outside (yellow) ezrin-rich regions (grayscale). Magnified trajectories of IgM (E) inside (red) and (F) outside (yellow) ezrin-rich regions demarcated by white lines.

(G) Diffusion coefficients of single molecules of BCR inside (circles) and outside (triangles) ezrin-rich areas with the median indicated by red bar.

(H) Relative frequencies of single molecules of BCR inside (circles) and outside (triangles) actin-rich areas with diffusion coefficients in the indicated bins.

observed (Figure S3). Given that these filopodial F-actin structures are distinct from the cell cortex, we excluded these structures from our analysis of the regulation of BCR diffusion dynamics.

To examine the diffusion of the BCR in relation to actin, we defined masks (Supplemental Experimental Procedures, Figure S4) based on the fluorescence intensity of Lifeact-GFP and plotted single-molecule tracks of at least 10 frames (500 ms) "inside" or "outside" actin-rich regions (Figures 3B–3D). We observed that the rate of diffusion is inversely related to the density of actin filaments, such that BCRs in actin-rich areas have reduced mobility while diffusion is increased in actin-poor regions. The median diffusion coefficient of IgM was decreased more than 50% inside actin-rich regions compared to outside actin-rich regions (0.014 $\mu m^2 s^{-1}$ compared with 0.039 $\mu m^2 s^{-1}$) (Figure 3E). This decrease reflected a substantial increase in the proportion of slow-diffusing BCR inside actin-rich regions (Figure 3F). Similar BCR behavior in relation to actin was observed in B cells settled on planar lipid bilayers containing ICAM-1 (data not shown). Importantly, the wild-type BCR rarely crossed actin-rich areas (Movie S3). In contrast, highly mobile molecules of the chimeric IgM-H2 BCR frequently traversed actin-rich regions (Figure 3G; Movie S4). Indeed, analysis of these tracks in relation to actin-rich regions revealed a marked decrease in the frequency of slow-diffusing IgM-H2 and a concomitant increase in the proportion of more mobile BCR (Figures 3H–3J). The median diffusion coefficient both inside and outside actin-rich regions was increased by more than 2-fold compared to wild-type IgM (inside, 0.048 $\mu m^2 s^{-1}$ compared with 0.014 $\mu m^2 s^{-1}$; outside, 0.108 $\mu m^2 s^{-1}$ compared with 0.039 $\mu m^2 s^{-1}$) (Figure 3I). Although IgM-H2 molecules with slower diffusion in actin-rich regions were observed, the proportion of these molecules was reduced by nearly 50% compared to wild-type IgM (compare Figures 3F and 3J). These results suggest that the actin cytoskeleton influences steady-state BCR dynamics by defining barriers that limit diffusion. Moreover, it is clear that the intracellular domain of Igβ makes a substantial contribution to the efficiency of actin-mediated restriction of BCR diffusion.

The Ezrin-Mediated Link between the Plasma Membrane and the Actin Cytoskeleton Regulates BCR Diffusion

Interestingly, although the majority of slow-diffusing BCR were observed in actin-rich regions, we also observed slow-diffusing BCR outside actin-rich regions. We reasoned that the linkage between components of the plasma membrane and underlying actin filaments might influence BCR dynamics. The ezrin-radixin-moesin (ERM) family proteins seem likely candidates to mediate such a linkage (Bretscher et al., 2002), so we expressed and visualized ezrin-GFP in B cells. Similar to that observed for actin, under steady-state conditions, ezrin-GFP forms an intricate network (Figure 4A). Interestingly, when simultaneously visualized, we found that although similar, the density of these two networks is not fully coincident (Figure 4A; Movie S5). This

***$p < 0.0001$. Scale bars represent 2 μm. 300 representative diffusion coefficients displayed from a total of 500–3000 from at least three independent experiments. See also Figure S5.

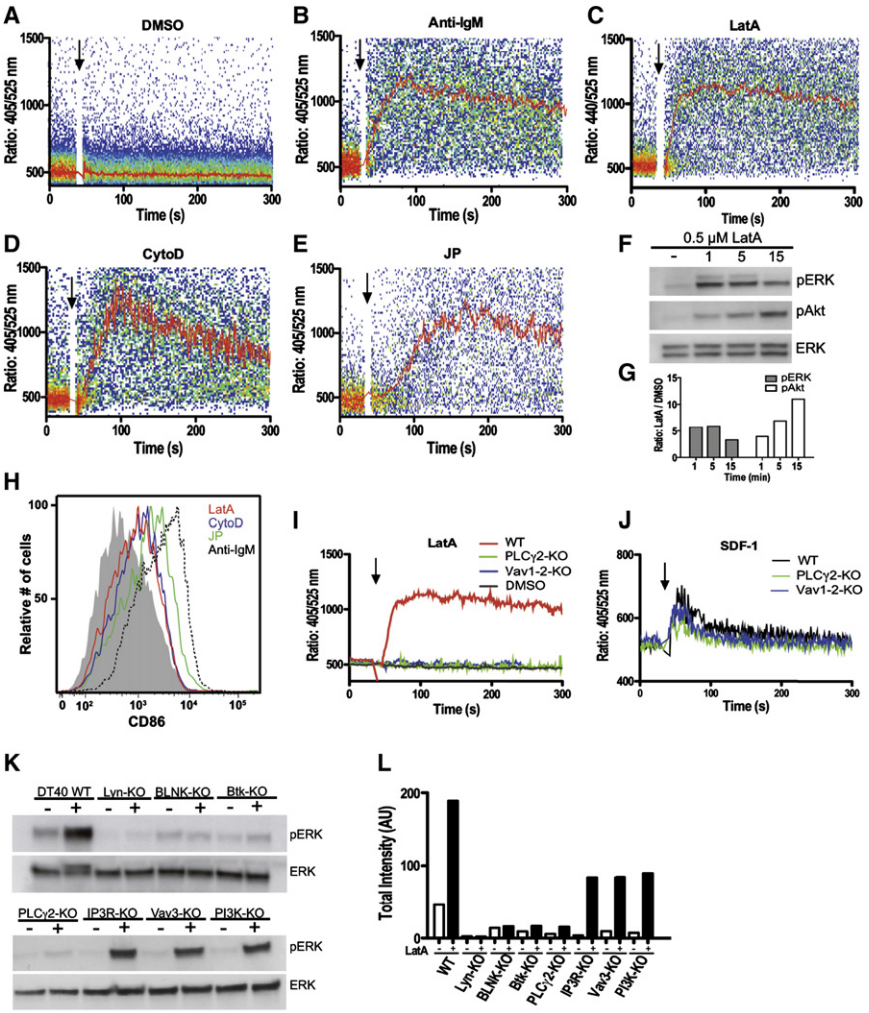

Figure 5. Alteration of the Actin Cytoskeleton Is Sufficient to Induce BCR Signaling

(A–H) Alteration of the actin cytoskeleton induces intracellular signaling.

(A–E) Ratiometric intracellular Ca^{2+} flux in primary naive B cells upon addition (indicated by black arrow) of vehicle control (DMSO) (A), 5 μg/ml anti-IgM F('ab)$_2$ (B), 0.5 μM LatA (C), 10 μM CytoD (D), or 1 μM JP (E) measured by flow cytometry. Mean indicated by red line.

(F) Primary naive B cells were treated with 0.5 μM LatA (+) or vehicle control (DMSO) (–) at 37°C for the indicated time. Cells were lysed and analyzed by SDS-PAGE followed by immunoblotting with anti-phospho-p44 and 42 MAPK (Erk1 and 2), anti-phospho-Akt, or anti-p44 and 42 MAPK.

(G) Quantification of the fold increase in pERK and pAkt upon LatA treatment.

(H) Primary naive B cells were treated or not (gray shaded) with 0.5 μM LatA (red line), 10 μM Cyto D (blue line), 1 μM JP (green line), or 5 μg/ml anti-IgM F('ab)$_2$ (black dotted line) for 5 min and then cultured for 24 hr. Cells were stained for the activation marker CD86 and analyzed by flow cytometry.

(I–L) Signaling induced by alteration of actin is predominantly mediated via the BCR. Ratiometric intracellular Ca^{2+} flux in primary wild-type (WT), PLCγ2-deficient, and Vav1 and 2 double-deficient B cells treated with 0.5 μM Lat A (I) or 200 ng/ml SDF-1 (J) measured by flow cytometry.

(K) Wild-type DT40 and various signaling-deficient cells including *Lyn*$^{-/-}$ (Lyn-KO), *Blnk*$^{-/-}$ (BLNK-KO), *Btk*$^{-/-}$ (Btk-KO), *Plcg2*$^{-/-}$ (PLCγ2-KO), *Itpr1*$^{-/-}$*Itpr2*$^{-/-}$*Itpr3*$^{-/-}$ (IP3R-KO), *Vav3*$^{-/-}$ (Vav3-KO), and *Pik3ca*$^{-/-}$ (PI3K-KO) were treated with 0.5 μM LatA or vehicle control (DMSO) for 5 min at 37°C. Cells were lysed and analyzed by SDS-PAGE followed by immunoblotting with anti-phospho-p44 and 42 MAPK (Erk1 and 2) and anti-p44 and 42 MAPK.

(L) Quantification of the induction of pERK upon LatA treatment shown in (K).

suggests that ezrin may mediate a membrane-cytoskeleton link not easily visualized under TIRF illumination. Furthermore, at the frame rate used for single-particle tracking, small dynamic "holes" in the ezrin network could be detected, suggesting that this protein rapidly regulates interactions between the actin cytoskeleton and the plasma membrane and thus may influence BCR diffusion (Figure 4B; Movie S5).

To investigate this role for ezrin, we visualized the distribution of ezrin-GFP together with the BCR. The BCR was largely slow moving, or confined, within ezrin-rich regions and more mobile in regions of reduced ezrin intensity (Figures 4C–4F; Movie S6). In contrast to actin, ezrin-GFP was more rapidly reorganized and appeared to create "gates" allowing the BCR to transition between compartments (Figure 4C; Figure S5, Movie S6). The median diffusion coefficient was three times slower inside ezrin-rich regions compared to outside ezrin-rich regions (0.011 $\mu m^2 s^{-1}$ compared with 0.037 $\mu m^2 s^{-1}$; Figure 4G), as a result of the markedly increased frequency of slow-diffusing BCR inside ezrin-rich regions (70% compared to 45%; Figure 4H). Moreover, we observed BCR confined in small spaces between ezrin-rich regions (Figure 4F), suggesting that the surrounding ezrin network limits BCR mobility. These results indicate that the ezrin-mediated linkage of the plasma membrane to actin filaments provides a mechanism for regulating steady-state BCR diffusion dynamics.

Alteration of the Actin Cytoskeleton Is Sufficient to Induce Signaling

To assess the functional significance of this ezrin- and actin-mediated restriction in BCR diffusion in steady-state B cells, we monitored intracellular calcium flux by flow cytometry upon treatment of cells with pharmacological agents of actin alteration. Latrunculin A (LatA) treatment is sufficient to induce robust calcium signaling comparable to that induced by crosslinking IgM (Figures 5A–5C). Similar results were obtained upon treatment of cells with the fungal toxin Cytochalasin D (CytoD), which binds to the barbed ends of actin filaments and thus disrupts actin polymerization (Figure 5D). Jasplakinolide (JP), an actin-stabilizing drug, in vitro also induced robust calcium signaling (Figure 5E). To determine whether alteration of the actin cytoskeleton was sufficient to induce other signaling pathways, we examined phosphorylation of downstream signaling molecules

including ERK and Akt. We observed a rapid induction of phosphorylation of these substrates upon disruption of the actin cytoskeleton (Figures 5F and 5G). Moreover, we detect upregulation of the activation marker CD86 1 day after a brief treatment of primary naive B cells with actin-disrupting agents (Figure 5H). Taken together, these results indicate that the signaling induced by disruption of the actin cytoskeleton is sufficient to induce not only early signaling events but also expression of costimulatory molecules. These observations suggest that the actin cytoskeleton plays an important role in regulating signaling in B cells.

Actin Alteration-Induced Signaling Is Probably Mediated by the BCR

Given that the BCR is among the most abundant cell surface receptor in naive B cells (~250,000/B cell, data not shown), we were keen to determine whether this signaling induced by actin alteration is mediated predominantly through the BCR. Indeed, calcium signaling upon disruption of the actin cytoskeleton with LatA is abrogated in primary naive B cells that lack key downstream regulators of BCR signaling, such as PLCγ2 and Vav (Figure 5I). Similar results were obtained upon treatment with CytoD and JP (data not shown). In contrast, no substantial difference in calcium signaling in response to the chemokine SDF-1 was observed in PLCγ2 or Vav1 and 2 deficient B cells compared to wild-type B cells (Figure 5J), demonstrating that the lack of calcium flux in these cells upon treatment with actin-disrupting agents is not simply due to an intrinsic defect in the calcium pathway. In order to genetically dissect this signaling pathway, we examined a panel of DT40 B cells deficient in a number of key signaling molecules. We observed that, consistent with primary naive murine B cells, treatment of DT40 B cells with LatA induced rapid phosphorylation of ERK (Figures 5K and 5L). In contrast, phosphorylation of ERK was abrogated in DT40 B cells lacking key BCR signaling molecules, including Lyn, BLNK, Btk, and PLCγ2 (Figures 5K and 5L). However, alteration of F-actin induced phosphorylation of ERK in IP3R-, Vav3-, and PI3K-deficient cells (Figures 5K and 5L), consistent with ERK activation upon BCR-crosslinking as previously reported (Fujikawa et al., 2003; Hashimoto et al., 1998; Okkenhaug et al., 2002). These results provide genetic evidence that alteration of the actin cytoskeleton induces signaling in steady-state B cells, which is probably mediated by the BCR.

Actin Alteration Increases BCR Diffusion

To gain insight into this actin-induced signaling, we assessed how alteration of the actin- and ezrin-defined membrane skeleton affected BCR diffusion. Treatment of Lifeact-GFP-expressing B cells with the actin-depolymerizing drugs LatA or CytoD was sufficient to observe a considerable disruption of the actin network, without drastic alteration of B cell morphology (Figure 6A; Movie S7). Somewhat surprisingly, treatment with JP also rapidly disrupted the actin cytoskeleton, as seen by the diminished intensity of Lifeact-GFP (Figure 6A; Movie S7). Biochemical analysis confirms the polymerization of F-actin after treatment with JP, consistent with the reported effect of JP. However, substantial alterations in the actin cytoskeleton upon treatment with JP were clearly observed by the increased intensity of Actin-GFP within patches at the membrane and intracellular regions via confocal microscopy (Figure S6). We treated naive primary murine B cells with these pharmacological agents to determine the effect of cytoskeleton alteration on BCR diffusion. LatA treatment immediately gives rise to a nearly 3-fold increase in the median diffusion coefficient of the BCR (0.032 $\mu m^2 s^{-1}$ to 0.086 $\mu m^2 s^{-1}$; Figures 6B and 6C), reflecting both a decrease in the slow-diffusing population and an increase in the faster-diffusing populations (Figure 6C). Similarly, treatment of B cells with CytoD caused a 3-fold increase in the median diffusion coefficient of the BCR (0.032 $\mu m^2 s^{-1}$ to 0.095 $\mu m^2 s^{-1}$; Figures 6B and 6C). BCR diffusion was also markedly increased upon treatment of B cells with JP (Figure 6B), which reflected a substantial reduction in the slow-diffusing population (Figure 6C). Interestingly, we also observed a nearly 10-fold increase in the median diffusion coefficient of IgD after treatment with LatA, indicating that the actin cytoskeleton is an important regulator of BCR diffusion independent of isotype (Figures 6D and 6E). In line with this, overexpression of a dominant-negative form of ezrin, which lacks the actin-binding domain (Ezrin-310) and therefore disrupts the linkage between the plasma membrane and actin filaments, increased the median BCR diffusion coefficient (Figure 6F). In contrast, overexpression of a constitutively active form of ezrin (Ezrin-TD) markedly decreased BCR diffusion (Figure 6G). Taken together, these results demonstrate that alteration of the membrane skeleton in steady-state B cells causes an increase in BCR diffusion, which may be linked to the induction of signaling.

BCR Diffusion Correlates with Signaling

In order to determine whether the observed signaling was related to the rate of BCR diffusion, we titrated the concentration of CytoD used to induce calcium signaling from 0.5 μM to 10 μM. We detected negligible calcium flux at the lowest concentration of CytoD and incremental increases in calcium flux from 2 μM to 10 μM (Figure 6H). We determined that a similar population of cells was fluxing calcium, but that the peak flux increased with increasing CytoD (data not shown). We also measured a concomitant increase in the median diffusion coefficient of the BCR with increasing concentrations of CytoD (Figure 6I). This increase reflected a step-wise decrease in the proportion of very-slow-diffusing BCR (far left peak of histogram) with increasing concentration of CytoD (Figure 6J). Thus, we found that increasing concentrations of CytoD resulted in a similar concomitant increase in calcium as well as in the proportion of mobile BCR. Moreover, we find a strong correlation between the integrated area under the calcium curve and the mobile fraction of the BCR (Figure 6K). These results suggest that the signaling induced upon alteration of the actin cytoskeleton may be related to changes in BCR diffusion dynamics.

BCR signaling after antigen engagement induces dramatic cytoskeleton reorganization (Arana et al., 2008; Fleire et al., 2006; Lin et al., 2008). Thus, it seems plausible that BCR expression alone might produce a low-intensity signal (Lam et al., 1997; Rajewsky, 1996) that may to some degree regulate steady-state actin organization or dynamics. In line with this, we observed that B cells deficient in Syk, one of the earliest tyrosine kinases activated upon BCR stimulation, had dramatically altered organization of the actin cytoskeleton (Figures 7A and 7B). Indeed, we observed an increased number of actin-rich filopodia in which linear diffusion of the BCR prevented us from further analysis

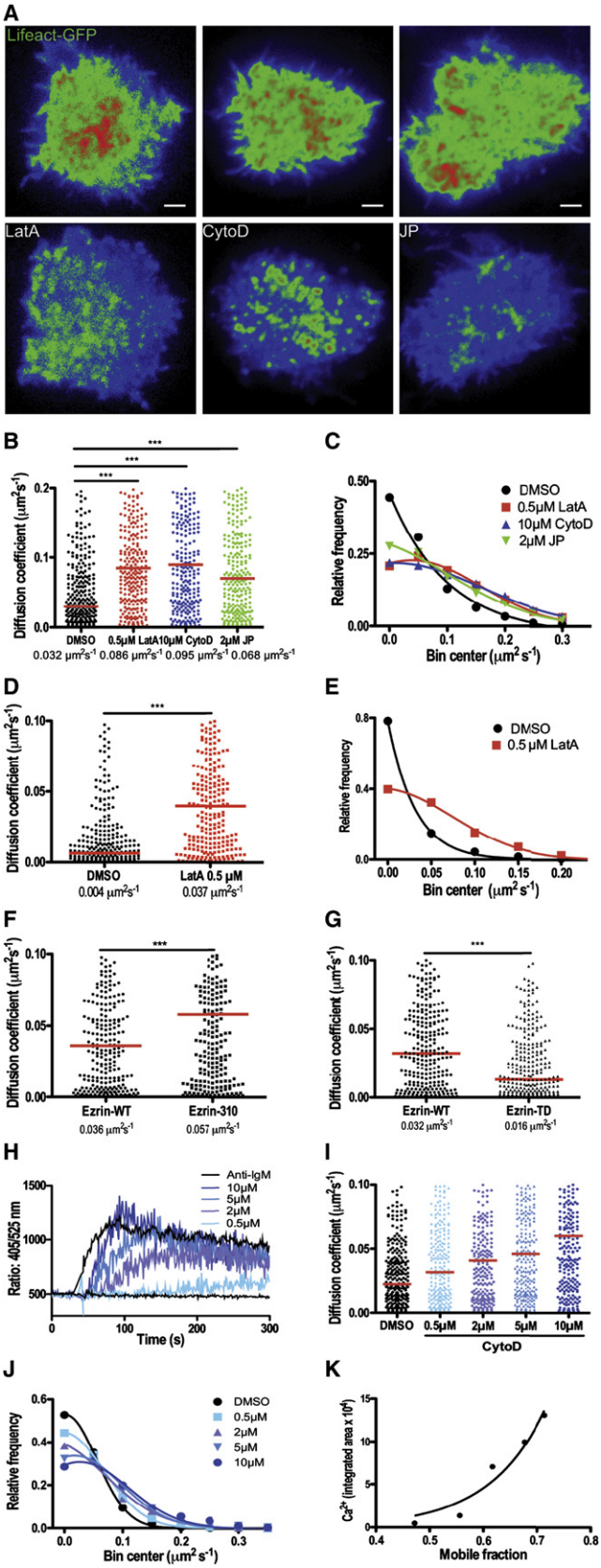

Figure 6. Signaling Induced by Disruption of Actin Correlates with BCR Diffusion

(A–E) Pharmacological agents of actin disruption increase BCR diffusion.

(A) Lifeact-GFP-expressing cells were visualized by TIRFM before (top) and 5 min after treatment (bottom) with 0.5 μM LatA, 10 μM CytoD, or 2 μM JP.

(B and C) Single-molecule tracking of IgM in primary naive B cells on MHC II-coated coverslips upon treatment with 0.5 μM LatA (red), 10 μM CytoD (blue), 2 μM JP (green), or vehicle control (DMSO; black). Diffusion coefficients with the median indicated in red (B) and distribution histogram (C) with diffusion coefficients in the indicated bins.

(D and E) Single-molecule tracking of IgD in primary naive B cells treated with 0.5 μM LatA (red squares) or vehicle control (black circles). Diffusion coefficients with the median indicated in red (D) and distribution histogram (E) with diffusion coefficients in the indicated bins.

(F and G) Genetic alteration of membrane-cytoskeleton link modifies BCR diffusion. Diffusion coefficients of single molecules of BCR in A20 B cells expressing wild-type ezrin-GFP (circles) and ezrin-310-GFP (squares) (F) or DT40 B cells expressing wild-type ezrin-GFP (circles) and ezrin-TD-GFP (squares) (G) with the median indicated in red.

(H–K) Increasing concentrations of CytoD increase intracellular calcium flux and the mobile fraction of the BCR.

(H) Ratiometric intracellular Ca^{2+} flux in primary naive B cells treated with 0.5–10 μM CytoD measured by flow cytometry.

(I and J) Diffusion coefficients (I) and distribution histogram (J) of single molecules of IgM in primary naive B cells upon treatment with increasing concentrations of CytoD.

(K) The integrated area under the calcium curve in (H) was plotted against the mobile fraction (all bins except lowest) of the BCR from (J).

***$p < 0.0001$. 300 representative diffusion coefficients displayed from a total of 500–3000 from at least two independent experiments. See also Figure S6.

of BCR diffusion in these cells (Figure S3). Similar results were observed in B cells deficient in the Src-family kinase Lyn (data not shown). Consistent with these observations, we found that treatment of primary naive B cells with the Syk inhibitor, Piceatannol, dramatically altered cell morphology (M.W. and F.D.B., unpublished). Nonetheless, we were able to measure BCR diffusion in primary naive B cells deficient in PLCγ2 and Vav1 and 2, where the actin network does not appear to be as substantially altered. We observed that IgM diffusion is decreased in both PLCγ2- and Vav1- and 2-deficient B cells (Figure 7C). This decrease reflected a 20% increase in the slow-diffusing population (Figure 7D). Taken together, these results suggest that perhaps tonic signaling through the BCR may also influence steady-state actin dynamics or organization (Figure S7). Such interplay between tonic BCR signaling and actin dynamics may provide a mechanism for regulating this low-level constitutive signaling.

DISCUSSION

By using dual-view TIRF acquisition, we were able to simultaneously measure the steady-state diffusion of the two BCR isotypes expressed by naive B cells. We observed that diffusion of both IgM and IgD is restricted within the plasma membrane. Interestingly, the proportion of BCR that was very slow diffusing was greater for IgD compared to IgM. The reason for the increased immobility of IgD has yet to be identified but may be due to the presence of both transmembrane and GPI-anchored forms, which could alter microdomain association (Chaturvedi et al., 2002; Wienands and Reth, 1992). Moreover, we previously observed that IgD appears to be preclustered (Depoil et al.,

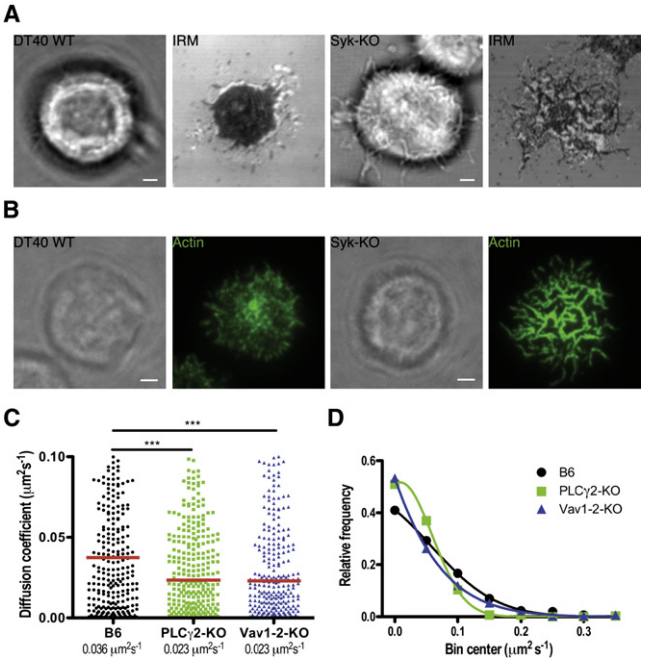

Figure 7. BCR Diffusion Is Decreased in B Cells Deficient in PLCγ2 and Vav1/2

(A and B) Signaling-deficient B cells have altered actin cytoskeleton.

(A) DT40 WT or Syk-deficient B cells were allowed to settle on fibronectin-coated coverslips and cell morphology and adhesion were examined by differential interference contrast (DIC) and interference reflection microscopy (IRM).

(B) DT40 WT and Syk-deficient B cells on fibronectin-coated coverslips were fixed and F-actin was stained with phalloidin and visualized by TIRFM.

Scale bars represent 2 μm.

(C and D) Signaling-deficient B cells have reduced IgM diffusion. Single-molecule tracking of IgM in primary naive B6 (black circle), PLCγ2-deficient (green square), and Vav1 and 2 double-deficient (blue triangle). Diffusion coefficients (C) and distribution histogram (D) with diffusion coefficients in the indicated bins. Median indicated by red line. ***$p < 0.0001$. 300 representative diffusion coefficients displayed from a total of 500–3000 from at least two independent experiments. See also Figure S7.

2008) and such organization could influence diffusion dynamics. Indeed, it should be noted that although we are able to visualize single particles of BCR, we do not know whether these particles are monomers or oligomers (Schamel and Reth, 2000) or even higher-order "protein islands" (Lillemeier et al., 2006).

We have identified the intracellular domain of Igβ as a crucial element for the restriction in BCR diffusion. Simply substituting the intracellular domain of Igβ with that of MHC class I increased BCR diffusion nearly 3-fold. The intracellular domain of Igβ and MHC class I do not differ greatly in size, particularly in comparison to the whole protein, so it is unlikely that the difference in diffusion is merely size-dependent slowing. Instead, our data suggest that Igβ increases the efficiency of actin-mediated restriction in BCR diffusion. It remains to be determined whether this is due to a specific interaction between Igβ and actin, or whether a difference in the length or tertiary structure of the cytoplasmic domain of Igβ and MHC class I affects their trapping by the membrane skeleton (Edidin et al., 1994). Also, it is possible that some of this difference in diffusion may be due to a difference in the net charge of the cytoplasmic domain, which could affect its affinity for proteins in the cytoplasm or electrostatic interactions with phospholipids in the plasma membrane (Xu et al., 2008). The very small difference between the IgM-Mutβ chimeric receptor and the diffusion dynamics of the wild-type receptor suggests that the transmembrane domain may also influence BCR diffusion, possibly through interaction with other proteins, such as CD19 and/or CD21 (Carter et al., 1997); the formation of BCR oligomers (Schamel and Reth, 2000); or microdomain association, which could influence additional factors such as molecular crowding (Dix and Verkman, 2008; Zhou, 2009).

A recent study examining the role of the extracellular Cμ4 domains in BCR clustering upon antigen stimulation noted that a proportion of BCR are immobile in unstimulated cells (Tolar et al., 2009). However, the mechanism or functional relevance of this observation was not investigated. Here, simultaneous visualization of two parameters has allowed us to investigate the mechanism that restricts steady-state BCR diffusion. We find that BCR diffusion is highly reduced within actin-rich regions, which may consist of membrane compartments on the nanometer scale as suggested by the membrane skeleton fence model (Kusumi et al., 2005). Moreover, we observe that this network defines micron-sized compartments, consistent with recent SPT observations of FcεRI in a basophilic cell line (Andrews et al., 2008). However, this work did not report highly restricted diffusion of FcεRI within actin-rich regions, so it remains to be determined whether our observations reflect a general phenomenon for ITAM-containing immunoreceptors.

Here we directly visualize how the dynamic linkage of the plasma membrane to the actin cytoskeleton influences diffusion. We identify the ERM protein ezrin as an important component regulating this interaction and defining BCR diffusion. We find that ezrin defines compartments or "corrals" that restrict diffusion as proposed in early models (Saxton, 1995; Sheetz, 1983; Sheetz et al., 1980). No doubt additional structural proteins of the membrane skeleton, such as gelsolin, villin, or spectrin, are likely to also participate in the regulation of diffusion. What's more, we observed rapid remodeling of the ezrin network and propose that ezrin provides a mechanism to very quickly modify membrane protein diffusion. Indeed, our visualization of ezrin while simultaneously tracking the BCR suggests that such proteins dynamically "gate" (Tsuji and Ohnishi, 1986) the diffusion of membrane proteins and may permit the transitional "hop" between compartments observed in previous SPT studies (Fujiwara et al., 2002; Kusumi et al., 1993). Moreover, receptor signaling could regulate such a linkage (Delon et al., 2001; Faure et al., 2004; Gupta et al., 2006) and thus fine tune diffusion dynamics during activation. We posit that antigen-engaged BCRs probably trigger a localized dephosphorylation of ERM proteins and detachment of the membrane skeleton, thus altering diffusion of unengaged BCR in close proximity, which may then gain accessibility to ligand or BCR microclusters.

Importantly, we find that gross alteration of the actin cytoskeleton is sufficient to trigger B cell signaling to a similar extent as BCR crosslinking. Moreover, we demonstrate that this signaling is most probably mediated via the BCR and is correlated with increased BCR diffusion. It is therefore conceivable that the steady-state dynamism of the actin cytoskeleton, that is, small constitutive alterations in the organization of F-actin, provides a mechanism to generate low-intensity tonic BCR signaling.

Such signals may then feedback into alterations of the actin cytoskeleton. Indeed, we know that ligand-induced BCR signaling rapidly alters the organization of F-actin (Hao and August, 2005). Thus, we suggest that tonic BCR signaling may influence actin organization and dynamics. In line with this, B cells lacking key BCR signaling molecules have dramatically altered steady-state morphology (Weber et al., 2008). Moreover, IgM diffusion is decreased in B cells deficient in PLCγ2 and Vav1 and 2. These results imply an interplay between BCR signaling and the actin cytoskeleton, which probably contributes to the regulation of tonic signaling in B cells.

At present, it is not clear how alteration of the actin cytoskeleton triggers BCR signaling. According to the oligomeric BCR complex model (Reth et al., 2000; Schamel and Reth, 2000), association of antigen with pre-existing BCR oligomers induces a disruption of the oligomeric complex permitting accessibility and phosphorylation of Igα-β and the activation of signaling. Perhaps the actin cytoskeleton has a role in maintaining this complex. Interestingly, recent electron microscopy studies have shown that the TCR exists within higher-order protein islands that are connected to the actin cytoskeleton and depend on it for their formation and/or maintenance (Lillemeier et al., 2006). It may be that the oligomeric BCR complex is linked to actin and alteration of F-actin causes a similar disruption to the oligomeric complex induced by antigen and thus triggers BCR signaling. Dynamic actin remodeling might then be important for subsequent internalization of active BCR from the cell surface resulting in signal termination, as previous studies have suggested (Stoddart et al., 2005). It has also been suggested that the BCR undergoes clustering and a conformational opening of Igα-β upon antigen binding, which is dependent on association of the BCR with distinct lipid domains (Tolar et al., 2005). It may be that disruption of the actin cytoskeleton alters the localization of BCR and lipid rafts, possibly bringing together these membrane domains.

However, our data suggest that signaling induced by disruption of actin may be related to a change in BCR diffusion. Two possible models can be envisaged to account for our results. One model is that the membrane skeleton restricts BCR mobility and may thus restrict the interaction between the BCR and coreceptors or activated signaling molecules. Disruption of the diffusion barrier increases the mobile fraction of the BCR and may thus increase the probability that the BCR will encounter an activated kinase or coreceptor such as CD19. Alternatively, it may be that the actin cytoskeleton affects the segregation of kinases or phosphatases from the BCR during the steady state. For example, the actin cytoskeleton may immobilize BCRs and phosphatases together and disruption of F-actin releases this inhibitory interaction as BCRs diffuse away. An important parameter to determine will be whether the number of cell surface BCRs alters the signaling induced by disruption of the actin cytoskeleton, as well as the location of tyrosine kinases, protein phosphatases, and coreceptors. Future research investigating the locations of these activating and inhibitory molecules in relation to actin may shed light on these potential models.

Our data provide convincing evidence that an ezrin- and actin-defined network influences steady-state BCR diffusion dynamics by creating barriers that restrict BCR diffusion. We identify the intracellular domain of Igβ as important for the efficiency of this restriction in BCR diffusion. Importantly, alteration of this network is sufficient to induce robust intracellular signaling, in the absence of antigen stimulation, which is concomitant with an increase in BCR mobility. Moreover, we show that this signaling is most probably initiated by the BCR. Thus, our results suggest that the membrane skeleton plays an important function in controlling BCR dynamics and thereby signaling in a way that could be important for understanding both tonic and antigen-induced signaling.

EXPERIMENTAL PROCEDURES

Cell Preparation and Culture

C57BL/6 wild-type mice, MD4 (HEL-specific BCR) (Goodnow et al., 1988), and *Plcg2*$^{fl/fl}$ *Cd19*Cre$^{+/-}$ mice (Hashimoto et al., 2000) were kindly provided by T. Kurosaki, RIKEN (Japan), and *Vav1*$^{-/-}$*Vav2*$^{-/-}$ mice (Doody et al., 2001), kindly provided by M. Turner, Babraham Institute (Cambridge, UK), were used. Splenic naive B cells were purified as described previously (Carrasco et al., 2004). This purification resulted in a population with 95%–98% B cells. Primary B cells and A20 B cells expressing IgM, IgM-H2, IgM-Mutβ (Williams et al., 1994) or Hel-H2, and Hel-Igβ were cultured in RPMI 1640 containing 10% FCS, penicillin and streptomycin antibiotics (Invitrogen, Carlsbad, CA), and 50 μM 2-mercaptoethanol (Sigma-Aldrich, St. Louis, MO). Wehi 231 (ATCC CRL-1702) B cells were cultured in DMEM supplemented with 10% FCS and 50 μM 2-mercaptoethanol. *Lyn*$^{-/-}$, *Blnk*$^{-/-}$, *Btk*$^{-/-}$, *Plcg2*$^{-/-}$, *Itpr1*$^{-/-}$*Itpr2*$^{-/-}$*Itpr3*$^{-/-}$, *Vav3*$^{-/-}$, *Pik3ca*$^{-/-}$, and WT DT40 cells were used (Shinohara and Kurosaki, 2006). DT40 cells were cultured at 39.5°C in RPMI 1640 containing 10% FCS, 1% chicken serum, penicillin and streptomycin antibiotics (Invitrogen), and 50 μM 2-mercaptoethanol (Sigma-Aldrich). All experiments were approved by the Cancer Research UK Animal Ethics Committee and the UK Home Office.

Cloning of Recombinant Lysozymes

For the generation of Hel-H2 and Hel-Igβ chimeras, Hel sequence was amplified by PCR from a pcDNA3 plasmid containing a Hel-cDNA fragment (Batista and Neuberger, 1998) with the sense primer 5′ CGGAATTCATGAGGTCTTTGC TAATC 3′ and antisense primer 5′ CGGGATCCAGATCCGCTTCCACC 3′ and cloned in the pCDNA3.1 expression vector in EcoRI and BamHI restriction sites. H2 and Igβ sheaths were amplified with pSV2gpt plasmids containing IgM-H2 or IgM-Igβ as templates described previously (Aluvihare et al., 1997). Fragments were amplified with the sense primer 5′ CGGGATCCCCTCCTC CATCCACT 3′ and the antisense primers 5′CGCCTTAAGTCACGCTAGAGAA TGAGG 3′ (HEL-H2) or 5′ GCGCTTAAGTCATTCCTGGCCTGG 3′ (HEL-Igβ) and cloned in the Hel-pCDNA3.1 vector in BamHI and AflII restriction sites.

Reagents

Latrunculin A, Cytochalasin D, and Jasplakinolide was purchased from Calbiochem. For BCR diffusion analysis, 0.5 μM LatA, 0.5–10 μM Cytochalasin D, or 1 μM Jasplakinolide prewarmed in PBS was injected into FCS2 chambers during imaging. Ezrin-GFP, Ezrin-310-GFP, and Ezrin-TD-GFP constructs were kind gifts from E. Sahai (London Research Institute, CRUK) (Sahai and Marshall, 2003). Lifeact-GFP and Lifeact-mRFPruby (Riedl et al., 2008) were kindly provided by M. Sixt (Max Plank Institute of Biochemistry, Munich).

Glass Coverslip Coating

Acid-cleaned glass coverslips were incubated with either 1 μg/ml of anti-MHCII (M5/114; ATCC TIB120) for 4 hr, 4 μg/ml (A20 B cells) or 0.5 μg/ml (DT40 B cells) fibronectin (Sigma-Aldrich) for 1 hr and washed with PBS.

Cell Labeling for Single-Particle Tracking

Primary naive and A20 B cells were labeled with Cy3-labeled goat anti-mouse IgM Fab fragment (Jackson Immunoresearch) or Cy3-labeled goat anti-mouse IgG Fab fragment (Jackson Immunoresearch), or unconjugated Fabs were labeled with AlexaFluor-555 (Molecular Probes) or Attotec 633 (Attotec) according to manufacturer's instructions. B cells were incubated with one of the following: 1 ng/ml of labeled anti-IgM mixed with 2 μg/ml of unlabeled

anti-IgM Fab (Jackson ImmunoResearch), 100 ng/ml of labeled anti-IgD Fab mixed with 4 μg/ml unlabeled anti-IgD Fab, 10 ng/ml of labeled anti-MHCII Fab mixed with 1 μg/ml of unlabeled anti-MHCII Fab, 160 ng/ml of labeled anti-MHCI mixed with 4 μg/ml unlabeled anti-MHCI, 80 ng/ml labeled anti-Hel mixed with 4 μg/ml unlabeled anti-Hel, or 600 ng/ml of labeled anti-chicken IgM Fab in chamber buffer for 15 min at 4°C, then washed with PBS.

Preparation of Fab Fragments of Monoclonal Antibodies

Fab fragments of purified monoclonal antibodies to murine IgD (11-26c), MHCII (M5/114; ATCC TIB120), MHCI (K918), Hel (D1.3), and chicken IgM (M1) were prepared as previously described (Depoil et al., 2008). Anti-IgD, anti-MHCII, and anti-chicken IgM were labeled with AlexaFluor dye according to manufacturer's instructions (Molecular Probes).

Calcium Flux by Flow Cytometry

Intracellular Ca^{2+} flux was measured by flow cytometry with a ratiometric indicator. Primary naive B cells were preloaded with 3 μM Indo-1 AM (Molecular Probes, Invitrogen) in RPMI at 37°C for 20 min. After collecting a baseline reading for 30 s, 0.5 μM LatA, 0.5–10 μM Cytochalasin D, 1 μM Jasplakinolide, 5 μg/ml anti-IgM $F(ab')_2$ (Jackson), or 200 ng/ml murine SDF-1α (Peprotech) was added to the facs tube, and the ratio of fluorescence (405/525 nm) was determined for 300 s with a LSRII cytometer (BD Biosciences).

Cell Stimulation and Immunoblotting

Primary naive, A20, and DT40 B cells were equilibrated in RPMI at 37°C for 10 min and then 0.5 μM LatA prewarmed in PBS was added for the indicated time. Cells were lysed in 2× Laemelli sample buffer and analyzed by SDS-PAGE followed by immunoblotting with anti-phospho-p44 and 42 MAPK (Erk1 and 2), anti-phospho-Akt, or anti-p44 and 42 MAPK (all from Cell Signaling).

G-Actin/F-Actin In Vivo Assay

Primary naive B cells were treated or not with 1 μM jasplakinolide for the indicated time, lysed, and fractionated according to the manufacturer's protocol (Cytoskeleton). Soluble and insoluble fractions were separated by SDS-PAGE and immunoblotted for mouse β-actin (Sigma). F-actin content was calculated by the total intensity of insoluble/(insoluble + soluble) fractions and is represented as a percentage.

Fluorescence Recovery after Photobleaching

Experiments were performed on a multiphoton microscope (Olympus Fluoview FV1000 MPE2 Twin system) with a 25× 1.05 NA water-immersion objective (Olympus XLPLNWMP) and Fluoview software. Fluorescence excitation and bleaching was performed with a pulsed Ti:sapphire laser at 890 nm (Spectra Physics MaiTai HP DeepSee). A small circular region was bleached for 50 ms with the tornado scanning option of the main scanner of the system. The high-speed scanning mode was used at 8 frames/s to record 10 frames before the bleaching event and to monitor fluorescence recovery for 100 frames afterwards.

Statistical Analysis

Frequency distribution analysis and the nonparametric Wilcoxon Mann-Whitney Test were performed on data with GraphPad Prism version 5.00 for Windows, GraphPad Software, San Diego, CA (http://www.graphpad.com).

Instrument

Single-molecule fluorescence microscopy was performed with an Olympus TIRFM system based on an inverted microscope (Olympus IX81), 150 × NA 1.45 TIRFM objective (Olympus), motorized filter wheel (Olympus), sensitive EMCCD camera (Cascade II, Photometrics), and real time data acquisition (Olympus, Cell∼R). Three laser lines (488 nm, 561 nm, and 635 nm) can be used simultaneously while TIRF illumination is individually adjusted with three separate TIRFM illumination combiners (Olympus). Simultaneous two-channel recording was accomplished by mounting an image splitter (Optosplit II, Cairn Research, Faversham, UK) and a second EMCCD camera (Quant EM 512SC, Photometrics) on the bottom port. Image acquisition for the second camera was recorded with Image-Pro Plus (Media Cybernetics). Image registration was achieved by measuring the position of fluorescent microspheres (TetraSpek 0.1 μm, Invitrogen).

Image Processing

Dual View TIRFM channels of actin or ezrin and BCR were split with the Cairn Image Splitter plugin of ImageJ (NIH, http://rsb.info.nih.gov.ij). Actin or Ezrin images for movie overlays were then time averaged (5 frames) (http://valelab.ucsf.edu/∼nico/IJplugins/), background subtracted (rolling ball size 15), and Gaussian filtered (1), all via ImageJ.

Single-Molecule Detection

For single-molecule imaging, an area of approximately 2300 μm^2 was illuminated by 3.5 mW laser power resulting in a power density of approximately 150 W/cm^2 out of the objective. From the size, intensity, and single-step or multistep photobleaching (Figure S1), we conclude that we are able to image single BCR molecules labeled with one or two fluorophores. Individual fluorophores show characteristic intensity fluctuations on the millisecond to second time scale (blinking) when the fluorophore converts to a transient dark state (data not shown; Aitken et al., 2008). Frame rates of 20 frames/s were used to record image sequences of 200 frames. The signal to noise ratio, defined as the peak intensity after background subtraction divided by the standard deviation of the background fluctuations, was measured on one experimental data set as 7.2 ± 0.6 (n = 10) (Bobroff, 1986).

SUPPLEMENTAL INFORMATION

Supplemental Information includes Supplemental Experimental Procedures, seven figures, and seven movies and can be found with this article online at doi:10.1016/j.immuni.2009.12.005.

ACKNOWLEDGMENTS

We thank T. Kurosaki for PLCγ2-deficient mice and M. Turner for Vav1 and 2 double-deficient mice. The authors would like to thank D. Coombs and R. Das for helpful discussions on single-particle analysis. We would also like to thank P. Mattila, N.E. Harwood, and E. Sahai for critically reading the manuscript and for helpful comments. This work was supported by Cancer Research UK and the Royal Society Wolfson Research Merit Award (F.D.B.). O.D. was supported by funding from National Science and Engineering Research Council of Canada and the Mathematics in Technology and Complex Systems National Centre of Excellence, Canada.

Received: July 24, 2009
Revised: November 17, 2009
Accepted: December 4, 2009
Published online: February 18, 2010

REFERENCES

Aitken, C.E., Marshall, R.A., and Puglisi, J.D. (2008). An oxygen scavenging system for improvement of dye stability in single-molecule fluorescence experiments. Biophys. J. *94*, 1826–1835.

Aluvihare, V.R., Khamlichi, A.A., Williams, G.T., Adorini, L., and Neuberger, M.S. (1997). Acceleration of intracellular targeting of antigen by the B-cell antigen receptor: Importance depends on the nature of the antigen-antibody interaction. EMBO J. *16*, 3553–3562.

Andrews, N.L., Lidke, K.A., Pfeiffer, J.R., Burns, A.R., Wilson, B.S., Oliver, J.M., and Lidke, D.S. (2008). Actin restricts FcepsilonRI diffusion and facilitates antigen-induced receptor immobilization. Nat. Cell Biol. *10*, 955–963.

Arana, E., Vehlow, A., Harwood, N.E., Vigorito, E., Henderson, R., Turner, M., Tybulewicz, V.L., and Batista, F.D. (2008). Activation of the small GTPase Rac2 via the B cell receptor regulates B cell adhesion and immunological-synapse formation. Immunity *28*, 88–99.

Baeker, T.R., Simons, E.R., and Rothstein, T.L. (1987). Cytochalasin induces an increase in cytosolic free calcium in murine B lymphocytes. J. Immunol. *138*, 2691–2697.

Batista, F.D., and Harwood, N.E. (2009). The who, how and where of antigen presentation to B cells. Nat. Rev. Immunol. *9*, 15–27.

Batista, F.D., and Neuberger, M.S. (1998). Affinity dependence of the B cell response to antigen: A threshold, a ceiling, and the importance of off-rate. Immunity *8*, 751–759.

Bobroff, N. (1986). Position measurement with a resolution and noise-limited instrument. Rev. Sci. Instrum. *57*, 1152–1157.

Braun, J., Hochman, P.S., and Unanue, E.R. (1982). Ligand-induced association of surface immunoglobulin with the detergent-insoluble cytoskeletal matrix of the B lymphocyte. J. Immunol. *128*, 1198–1204.

Bretscher, A., Edwards, K., and Fehon, R.G. (2002). ERM proteins and merlin: Integrators at the cell cortex. Nat. Rev. Mol. Cell Biol. *3*, 586–599.

Carrasco, Y.R., Fleire, S.J., Cameron, T., Dustin, M.L., and Batista, F.D. (2004). LFA-1/ICAM-1 interaction lowers the threshold of B cell activation by facilitating B cell adhesion and synapse formation. Immunity *20*, 589–599.

Carter, R.H., Doody, G.M., Bolen, J.B., and Fearon, D.T. (1997). Membrane IgM-induced tyrosine phosphorylation of CD19 requires a CD19 domain that mediates association with components of the B cell antigen receptor complex. J. Immunol. *158*, 3062–3069.

Charrier, C., Ehrensperger, M.V., Dahan, M., Lévi, S., and Triller, A. (2006). Cytoskeleton regulation of glycine receptor number at synapses and diffusion in the plasma membrane. J. Neurosci. *26*, 8502–8511.

Chaturvedi, A., Siddiqui, Z., Bayiroglu, F., and Rao, K.V. (2002). A GPI-linked isoform of the IgD receptor regulates resting B cell activation. Nat. Immunol. *3*, 951–957.

DeFranco, A.L. (1997). The complexity of signaling pathways activated by the BCR. Curr. Opin. Immunol. *9*, 296–308.

Delon, J., Kaibuchi, K., and Germain, R.N. (2001). Exclusion of CD43 from the immunological synapse is mediated by phosphorylation-regulated relocation of the cytoskeletal adaptor moesin. Immunity *15*, 691–701.

Depoil, D., Fleire, S., Treanor, B.L., Weber, M., Harwood, N.E., Marchbank, K.L., Tybulewicz, V.L., and Batista, F.D. (2008). CD19 is essential for B cell activation by promoting B cell receptor-antigen microcluster formation in response to membrane-bound ligand. Nat. Immunol. *9*, 63–72.

Dix, J.A., and Verkman, A.S. (2008). Crowding effects on diffusion in solutions and cells. Annu Rev Biophys *37*, 247–263.

Doody, G.M., Bell, S.E., Vigorito, E., Clayton, E., McAdam, S., Tooze, R., Fernandez, C., Lee, I.J., and Turner, M. (2001). Signal transduction through Vav-2 participates in humoral immune responses and B cell maturation. Nat. Immunol. *2*, 542–547.

Douglass, A.D., and Vale, R.D. (2005). Single-molecule microscopy reveals plasma membrane microdomains created by protein-protein networks that exclude or trap signaling molecules in T cells. Cell *121*, 937–950.

Edidin, M., Zúñiga, M.C., and Sheetz, M.P. (1994). Truncation mutants define and locate cytoplasmic barriers to lateral mobility of membrane glycoproteins. Proc. Natl. Acad. Sci. USA *91*, 3378–3382.

Faure, S., Salazar-Fontana, L.I., Semichon, M., Tybulewicz, V.L., Bismuth, G., Trautmann, A., Germain, R.N., and Delon, J. (2004). ERM proteins regulate cytoskeleton relaxation promoting T cell-APC conjugation. Nat. Immunol. *5*, 272–279.

Fleire, S.J., Goldman, J.P., Carrasco, Y.R., Weber, M., Bray, D., and Batista, F.D. (2006). B cell ligand discrimination through a spreading and contraction response. Science *312*, 738–741.

Fujikawa, K., Miletic, A.V., Alt, F.W., Faccio, R., Brown, T., Hoog, J., Fredericks, J., Nishi, S., Mildiner, S., Moores, S.L., et al. (2003). Vav1/2/3-null mice define an essential role for Vav family proteins in lymphocyte development and activation but a differential requirement in MAPK signaling in T and B cells. J. Exp. Med. *198*, 1595–1608.

Fujiwara, T., Ritchie, K., Murakoshi, H., Jacobson, K., and Kusumi, A. (2002). Phospholipids undergo hop diffusion in compartmentalized cell membrane. J. Cell Biol. *157*, 1071–1081.

Fukatsu, K., Bannai, H., Zhang, S., Nakamura, H., Inoue, T., and Mikoshiba, K. (2004). Lateral diffusion of inositol 1,4,5-trisphosphate receptor type 1 is regulated by actin filaments and 4.1N in neuronal dendrites. J. Biol. Chem. *279*, 48976–48982.

Goodnow, C.C., Crosbie, J., Adelstein, S., Lavoie, T.B., Smith-Gill, S.J., Brink, R.A., Pritchard-Briscoe, H., Wotherspoon, J.S., Loblay, R.H., Raphael, K., et al. (1988). Altered immunoglobulin expression and functional silencing of self-reactive B lymphocytes in transgenic mice. Nature *334*, 676–682.

Gupta, N., Wollscheid, B., Watts, J.D., Scheer, B., Aebersold, R., and DeFranco, A.L. (2006). Quantitative proteomic analysis of B cell lipid rafts reveals that ezrin regulates antigen receptor-mediated lipid raft dynamics. Nat. Immunol. *7*, 625–633.

Haggie, P.M., Kim, J.K., Lukacs, G.L., and Verkman, A.S. (2006). Tracking of quantum dot-labeled CFTR shows near immobilization by C-terminal PDZ interactions. Mol. Biol. Cell *17*, 4937–4945.

Hao, S., and August, A. (2005). Actin depolymerization transduces the strength of B-cell receptor stimulation. Mol. Biol. Cell *16*, 2275–2284.

Hartwig, J.H., Jugloff, L.S., De Groot, N.J., Grupp, S.A., and Jongstra-Bilen, J. (1995). The ligand-induced membrane IgM association with the cytoskeletal matrix of B cells is not mediated through the Ig alpha beta heterodimer. J. Immunol. *155*, 3769–3779.

Hashimoto, A., Okada, H., Jiang, A., Kurosaki, M., Greenberg, S., Clark, E.A., and Kurosaki, T. (1998). Involvement of guanosine triphosphatases and phospholipase C-gamma2 in extracellular signal-regulated kinase, c-Jun NH2-terminal kinase, and p38 mitogen-activated protein kinase activation by the B cell antigen receptor. J. Exp. Med. *188*, 1287–1295.

Hashimoto, A., Takeda, K., Inaba, M., Sekimata, M., Kaisho, T., Ikehara, S., Homma, Y., Akira, S., and Kurosaki, T. (2000). Cutting edge: Essential role of phospholipase C-gamma 2 in B cell development and function. J. Immunol. *165*, 1738–1742.

Kurosaki, T. (2002). Regulation of B-cell signal transduction by adaptor proteins. Nat. Rev. Immunol. *2*, 354–363.

Kusumi, A., Sako, Y., and Yamamoto, M. (1993). Confined lateral diffusion of membrane receptors as studied by single particle tracking (nanovid microscopy). Effects of calcium-induced differentiation in cultured epithelial cells. Biophys. J. *65*, 2021–2040.

Kusumi, A., Nakada, C., Ritchie, K., Murase, K., Suzuki, K., Murakoshi, H., Kasai, R.S., Kondo, J., and Fujiwara, T. (2005). Paradigm shift of the plasma membrane concept from the two-dimensional continuum fluid to the partitioned fluid: high-speed single-molecule tracking of membrane molecules. Annu. Rev. Biophys. Biomol. Struct. *34*, 351–378.

Lam, K.P., Kühn, R., and Rajewsky, K. (1997). In vivo ablation of surface immunoglobulin on mature B cells by inducible gene targeting results in rapid cell death. Cell *90*, 1073–1083.

Lenne, P.F., Wawrezinieck, L., Conchonaud, F., Wurtz, O., Boned, A., Guo, X.J., Rigneault, H., He, H.T., and Marguet, D. (2006). Dynamic molecular confinement in the plasma membrane by microdomains and the cytoskeleton meshwork. EMBO J. *25*, 3245–3256.

Lillemeier, B.F., Pfeiffer, J.R., Surviladze, Z., Wilson, B.S., and Davis, M.M. (2006). Plasma membrane-associated proteins are clustered into islands attached to the cytoskeleton. Proc. Natl. Acad. Sci. USA *103*, 18992–18997.

Lin, K.B., Freeman, S.A., Zabetian, S., Brugger, H., Weber, M., Lei, V., Dang-Lawson, M., Tse, K.W., Santamaria, R., Batista, F.D., and Gold, M.R. (2008). The rap GTPases regulate B cell morphology, immune-synapse formation, and signaling by particulate B cell receptor ligands. Immunity *28*, 75–87.

Okkenhaug, K., Bilancio, A., Farjot, G., Priddle, H., Sancho, S., Peskett, E., Pearce, W., Meek, S.E., Salpekar, A., Waterfield, M.D., et al. (2002). Impaired B and T cell antigen receptor signaling in p110delta PI 3-kinase mutant mice. Science *297*, 1031–1034.

Rajewsky, K. (1996). Clonal selection and learning in the antibody system. Nature *381*, 751–758.

Reth, M. (1989). Antigen receptor tail clue. Nature *338*, 383–384.

Reth, M., Wienands, J., and Schamel, W.W. (2000). An unsolved problem of the clonal selection theory and the model of an oligomeric B-cell antigen receptor. Immunol. Rev. *176*, 10–18.

Riedl, J., Crevenna, A.H., Kessenbrock, K., Yu, J.H., Neukirchen, D., Bista, M., Bradke, F., Jenne, D., Holak, T.A., Werb, Z., et al. (2008). Lifeact: A versatile marker to visualize F-actin. Nat. Methods *5*, 605–607.

Sahai, E., and Marshall, C.J. (2003). Differing modes of tumour cell invasion have distinct requirements for Rho/ROCK signalling and extracellular proteolysis. Nat. Cell Biol. *5*, 711–719.

Saxton, M.J. (1993). Lateral diffusion in an archipelago. Single-particle diffusion. Biophys. J. *64*, 1766–1780.

Saxton, M.J. (1995). Single-particle tracking: Effects of corrals. Biophys. J. *69*, 389–398.

Schamel, W.W., and Reth, M. (2000). Monomeric and oligomeric complexes of the B cell antigen receptor. Immunity *13*, 5–14.

Sheetz, M.P. (1983). Membrane skeletal dynamics: Role in modulation of red cell deformability, mobility of transmembrane proteins, and shape. Semin. Hematol. *20*, 175–188.

Sheetz, M.P., Schindler, M., and Koppel, D.E. (1980). Lateral mobility of integral membrane proteins is increased in spherocytic erythrocytes. Nature *285*, 510–511.

Shinohara, H., and Kurosaki, T. (2006). Genetic analysis of B cell signaling. Subcell. Biochem. *40*, 145–187.

Stoddart, A., Jackson, A.P., and Brodsky, F.M. (2005). Plasticity of B cell receptor internalization upon conditional depletion of clathrin. Mol. Biol. Cell *16*, 2339–2348.

Suzuki, K., Ritchie, K., Kajikawa, E., Fujiwara, T., and Kusumi, A. (2005). Rapid hop diffusion of a G-protein-coupled receptor in the plasma membrane as revealed by single-molecule techniques. Biophys. J. *88*, 3659–3680.

Tang, Q., and Edidin, M. (2003). Lowering the barriers to random walks on the cell surface. Biophys. J. *84*, 400–407.

Tolar, P., Sohn, H.W., and Pierce, S.K. (2005). The initiation of antigen-induced B cell antigen receptor signaling viewed in living cells by fluorescence resonance energy transfer. Nat. Immunol. *6*, 1168–1176.

Tolar, P., Hanna, J., Krueger, P.D., and Pierce, S.K. (2009). The constant region of the membrane immunoglobulin mediates B cell-receptor clustering and signaling in response to membrane antigens. Immunity *30*, 44–55.

Tsuji, A., and Ohnishi, S. (1986). Restriction of the lateral motion of band 3 in the erythrocyte membrane by the cytoskeletal network: Dependence on spectrin association state. Biochemistry *25*, 6133–6139.

Umemura, Y.M., Vrljic, M., Nishimura, S.Y., Fujiwara, T.K., Suzuki, K.G., and Kusumi, A. (2008). Both MHC class II and its GPI-anchored form undergo hop diffusion as observed by single-molecule tracking. Biophys. J. *95*, 435–450.

Vrljic, M., Nishimura, S.Y., Brasselet, S., Moerner, W.E., and McConnell, H.M. (2002). Translational diffusion of individual class II MHC membrane proteins in cells. Biophys. J. *83*, 2681–2692.

Vrljic, M., Nishimura, S.Y., Moerner, W.E., and McConnell, H.M. (2005). Cholesterol depletion suppresses the translational diffusion of class II major histocompatibility complex proteins in the plasma membrane. Biophys. J. *88*, 334–347.

Wade, W.F., Freed, J.H., and Edidin, M. (1989). Translational diffusion of class II major histocompatibility complex molecules is constrained by their cytoplasmic domains. J. Cell Biol. *109*, 3325–3331.

Weber, M., Treanor, B., Depoil, D., Shinohara, H., Harwood, N.E., Hikida, M., Kurosaki, T., and Batista, F.D. (2008). Phospholipase C-gamma2 and Vav cooperate within signaling microclusters to propagate B cell spreading in response to membrane-bound antigen. J. Exp. Med. *205*, 853–868.

Wheeler, D., Sneddon, W.B., Wang, B., Friedman, P.A., and Romero, G. (2007). NHERF-1 and the cytoskeleton regulate the traffic and membrane dynamics of G protein-coupled receptors. J. Biol. Chem. *282*, 25076–25087.

Wienands, J., and Reth, M. (1992). Glycosyl-phosphatidylinositol linkage as a mechanism for cell-surface expression of immunoglobulin D. Nature *356*, 246–248.

Williams, G.T., Peaker, C.J., Patel, K.J., and Neuberger, M.S. (1994). The alpha/beta sheath and its cytoplasmic tyrosines are required for signaling by the B-cell antigen receptor but not for capping or for serine/threonine-kinase recruitment. Proc. Natl. Acad. Sci. USA *91*, 474–478.

Xu, C., Gagnon, E., Call, M.E., Schnell, J.R., Schwieters, C.D., Carman, C.V., Chou, J.J., and Wucherpfennig, K.W. (2008). Regulation of T cell receptor activation by dynamic membrane binding of the CD3epsilon cytoplasmic tyrosine-based motif. Cell *135*, 702–713.

Zhou, H.X. (2009). Crowding effects of membrane proteins. J. Phys. Chem. B *113*, 7995–8005.